Three-Dimensional Imaging Laser Radars with Geiger-Mode Avalanche Photodiode Arrays

Marius A. Albota, Brian F. Aull, Daniel G. Fouche, Richard M. Heinrichs, David G. Kocher, Richard M. Marino, James G. Mooney, Nathan R. Newbury, Michael E. O'Brien, Brian E. Player, Berton C. Willard, and John J. Zayhowski

Lincoln Laboratory is developing three-dimensional (3D) imaging laser radars (ladars) that feature few-centimeter range resolution, thousands of pixels, and capture of an entire 3D image on a single laser pulse. The transmitters are based on diode-pumped solid-state microchip lasers that are passively *Q*-switched. The receivers are based on microelectronic arrays of avalanche photodiodes (APDs) operating in Geiger (photon counting) mode, with integrated timing circuitry for each pixel. Ladars using these laser and detector technologies offer not only high performance, but also compact packaging, ruggedness, and high efficiency. Potential applications include advanced interceptor seekers, combat identification, navigation of autonomous robots and vehicles, surveillance, and topography. Early experiments with a single detector showed the feasibility of using a Geiger-mode APD for 3D imaging. Subsequently, we constructed a first-generation ("brassboard") 3D ladar incorporating a 4 × 4 array of Geiger-mode APDs and a microchip laser. Experiments with the brassboard and a low-light-level camera showed that in some important situations targets can be better detected and identified from 3D ladar images than from intensity images. We present results from both the single-detector and brassboard experiments.

Lincoln Laboratory is developing three-dimensional (3D) laser radars (ladars) with attractive features that include capture of an entire 3D image with a single laser pulse, image resolution of tens of thousands of pixels, range resolution of a few centimeters, and small size. The laser technology for the ladar is based on diode-pumped solid-state microchip lasers that are passively *Q*-switched [1]. The detector technology is based on arrays of avalanche photodiodes (APDs) operating in Geiger mode, with integrated timing circuitry for each pixel [2]. (In Geiger mode, an electron-hole pair generated by a single photon initiates an avalanche process that results in a large current pulse.)

Figure 1 shows the 3D ladar concept. Light from a single laser pulse is diverged to illuminate the entire scene of interest. An auxiliary detector marks the time at which the laser pulse is emitted. The reflected light is imaged onto a two-dimensional array of detectors. Rather than measuring intensity, as in a normal camera, these detectors measure the time of flight of the reflected light. The time of flight is proportional to

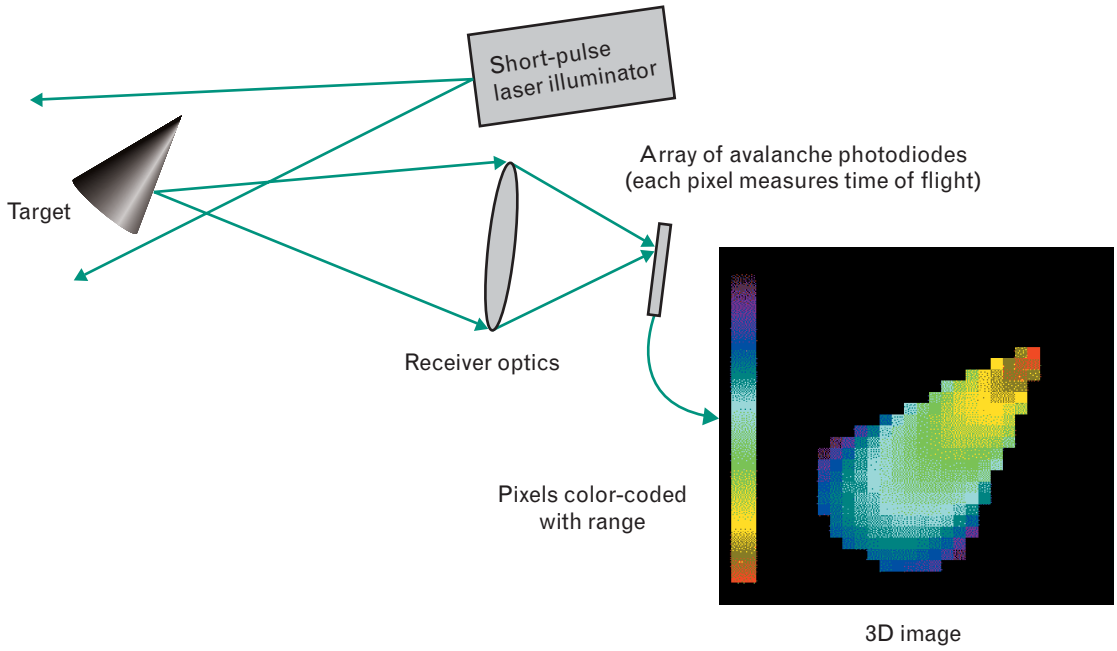

FIGURE 1. Concept for three-dimensional (3D) laser radar (ladar) that creates a 3D (angle-angle-range) image from a single laser pulse. The architecture for this active sensor is simple. A short-pulse laser is used to flood-illuminate the target scene. The receiver collects the backscattered light and directs an image of the target scene onto a two-dimensional array of avalanche photodiodes (APDs). Each pixel of the array measures the range to its associated target surface element by measuring the laser pulse two-way time of flight.

the distance between the point of reflection on the target and the sensor system. With range measured for each pixel, the ladar produces a 3D (angle-angle-range) image.

Discrimination and aimpoint selection for advanced interceptor seekers are potential applications for this type of ladar. The ladar is also well suited for combat identification, navigation of autonomous vehicles and robots, surveillance, and topography. In addition, as demonstrated by the 3D images shown in this article, the ladar can be used to find targets hidden by camouflage nets and foliage.

In this article, we provide a brief history of this effort and a description of more recent laser and detector technologies; detailed information is available elsewhere [1–13]. Next we describe a transportable "brassboard," or first-generation, 3D ladar that incorporates a microchip laser and a Geiger-mode APD array, and we show a few example images. Last, we show brassboard images of vehicles hidden by a camouflage net or trees. The 3D images are compared with those from a low-light-level intensity camera.

Advanced Discriminating Interceptor Seekers

In 1990, the Ballistic Missile Defense Organization (BMDO) initiated a series of programs to investigate the utility and feasibility of small ladars, which could be integral to future advanced discriminating interceptor seekers. The additional information provided by ladar technology was thought necessary to discriminate a warhead target from advanced and sophisticated decoys. The goal was to design a seeker system that featured both a passive infrared imaging sensor with a wide field of view and a high-resolution ladar sensor with a narrow field of view. A variety of ladar architectures and designs were investigated with competing teams. These included coherent mode-locked pulse-train ladars that could measure high-resolution range-Doppler images. The mode-locked waveform was investigated with both CO_2 (carbon dioxide) gas waveguide and solid-state Nd:YAG (neodymium-doped yttrium aluminum garnet) lasers operating at 10.6-μm and 1.06-μm wavelengths, respectively. Also studied was a direct-detection system

that illuminated the target scene with a short-pulse, solid-state, frequency-doubled Nd:YAG laser and split the receive signal into two channels. One channel was for a visible charge-coupled device (CCD) imager for high-resolution angle-angle-intensity data; the other was for a single fast APD detector to measure pulse-height intensity and range to target via time of flight.

We provided an independent analysis and assessment of the expected performance of these various ladar designs. Both coherent heterodyne and direct-detection sensor designs could provide high-resolution range data. Like the wideband coherent CO_2 ladar demonstrated earlier at Lincoln Laboratory's Firepond Infrared Research Facility in Westford, Massachusetts [3], the coherent heterodyne architectures also provided exquisite Doppler or velocity information. But these architectures were somewhat more complicated and heavier than the direct-detection sensor designs, which could also provide angle-angle-intensity data. One of the most stressing requirements for this advanced seeker was to make discrimination-supporting measurements as early as possible to allow enough time to divert and intercept the selected target. The sensor's maximum effective ranges were largely determined by the need to fit within the strict weight, volume, and size limits of the ladar design.

During these studies, it became clear that an alternate architecture has distinct merits. Our analysis showed that a direct-detection ladar that transmits short pulses and receives the backscattered signal by using a two-dimensional focal-plane array of photon-counting Geiger-mode APDs can measure the 3D spatial structure of a remote object [5]. The advantages of this design include the simplicity of a single-channel direct-detection receiver and the potential for extremely high sensitivity. In fact, when the effects of coherent interference (intensity variations due to speckle) are accounted for, photon counting with incoherent direct-detection systems can have superior detection statistics over those of coherent heterodyne systems. Furthermore, when APDs are operated in Geiger mode, they behave like binary or digital devices, and subsequent signal processing can be greatly simplified with this photon-to-digital converter.

Our analysis also showed that for a given laser-power-times-aperture-area product, 3D imaging with Geiger-mode APD arrays can provide important discrimination information at ranges greater than the other approaches being evaluated. Subsequent laboratory experiments verified the feasibility of high-resolution ranging with photon-counting Geiger-mode APD arrays. Lincoln Laboratory later embarked on a program to develop 4 × 4 and 32 × 32 arrays of silicon (Si) Geiger-mode detectors. Recently, these detectors have been successfully bonded to arrays of digital complementary-metal-oxide-semiconductor (CMOS) timing circuits. This unique detector technology is described in more detail in a companion article in this issue by B.F. Aull et al., entitled "Geiger-Mode Avalanche Photodiodes for Three-Dimensional Imaging" [2]. While this sensor technology still has application to advanced discriminating interceptor seekers, it also shows great promise for many other military and commercial applications.

Initial Feasibility Experiments

The idea of operating a photodiode with a bias voltage above its breakdown voltage and counting photons differs significantly from linear sensor concepts. Consequently, the first experiments were designed to compare linear versus Geiger-mode operation of a single avalanche photodiode. Figure 2 shows a dual-mode photon-counting detector device that was developed by EG&G Canada for this purpose. It includes an active quenching circuit to limit the current of the Geiger-mode avalanche and to reset the detector within 15 nsec. Figure 3 shows an example of a transistor-transistor logic (TTL) pulse triggered by the Geiger-mode detection of a single photon. Although the pulse width is approximately 10 nsec, jitter in the leading edge is what determines the ranging precision and effective resolution. Laboratory experiments demonstrated range precision of under 3 cm.

We developed a laboratory experiment to investigate the performance of single-photon ranging and to validate the concept of 3D imaging with Geiger-mode APDs. Test were performed with various Si Geiger-mode detector arrays from Radiation Monitoring Devices, Inc. The setup included a Lincoln Laboratory–developed short-pulse (<1 nsec), fre-

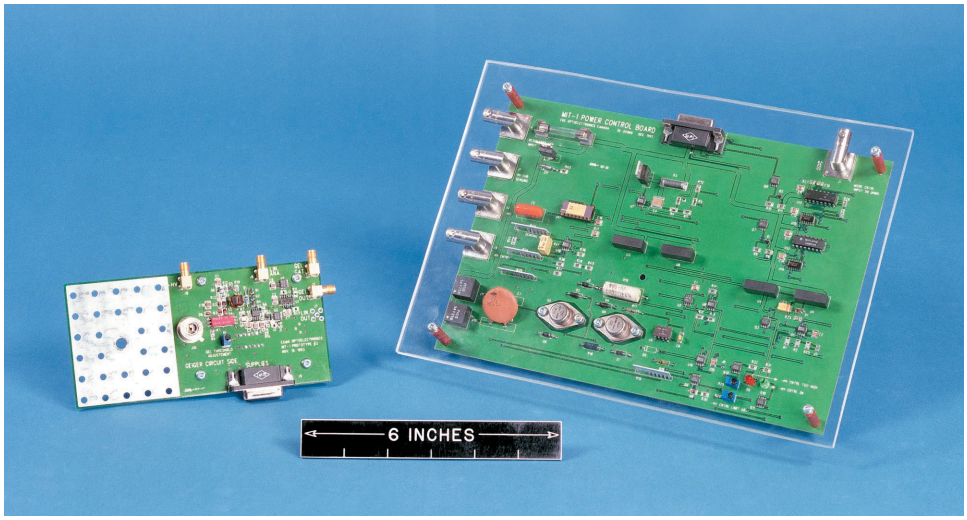

FIGURE 2. An early photon-counting detector system used to compare linear versus Geiger-mode operation of a single silicon (Si) APD. At left is a dual-mode single-element detector module, which includes an active-quenching circuit that can reset the Geiger-mode detector within 15 nsec. The detector could be operated in either a linear or a Geiger mode. In Geiger mode, the output of the APD was used to trigger a digital transistor-transistor-logic (TTL) pulse. At right is a control module used to set and control the detector operating conditions.

quency-doubled, Nd:YAG, microchip laser transmitting at 532-nm wavelength. The laser transmitter was used to flood-illuminate the scene, while the receiver field of view was scanned to generate a 32 × 32-pixel image of a variety of test objects. Figure 4 shows a diagram of the laboratory setup. Figure 5 shows example 3D ladar images of a cone with two spheres in the background. These are false color images, with the red end of the spectrum denoting the closest points in the scene and the blue end the most distant points. Figure 5 also shows image segmentation based on range. A simple thresholding operation separates foreground objects from background objects. Accomplishing such segmentation with a conventional intensity image would be much more difficult, especially if reflectivity contrast was low.

Figure 6 compares angle-angle-intensity images from a low-noise CCD with 3D spatial angle-angle-range images, all based on the scene consisting of a cone and two spheres shown in Figure 5. Both sets of images were generated by using the same illumination laser. The CCD pixels were binned to make a 32 × 32-pixel image to facilitate a fair comparison. Note that even with an estimated 700 received photons per frame (about 0.7 photon per pixel), recognizable objects begin to emerge in the image. Even with ten or a hundred times as many received photons per frame, it is difficult to recognize any of the objects in the intensity image.

These early experiments verified the utility of the photon-counting Geiger-mode APD as a unique

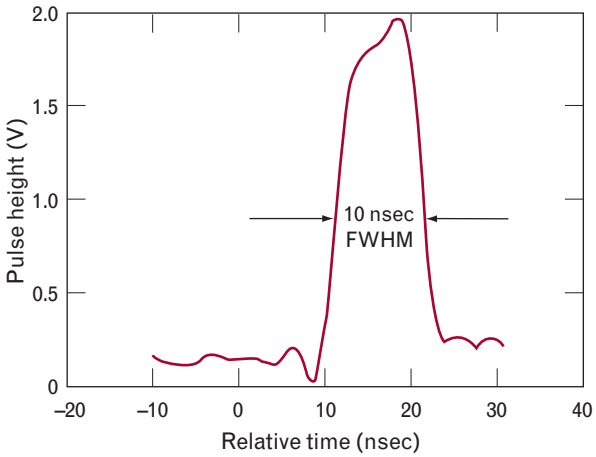

FIGURE 3. A TTL pulse generated by the Geiger-mode detection of a single photon. Jitter in the leading edge of the pulse width determines the range measurement precision. While the TTL pulse width is approximately 10 nsec full width half maximum (FWHM), the pulse-to-pulse jitter in the leading edge is less than 200 psec.

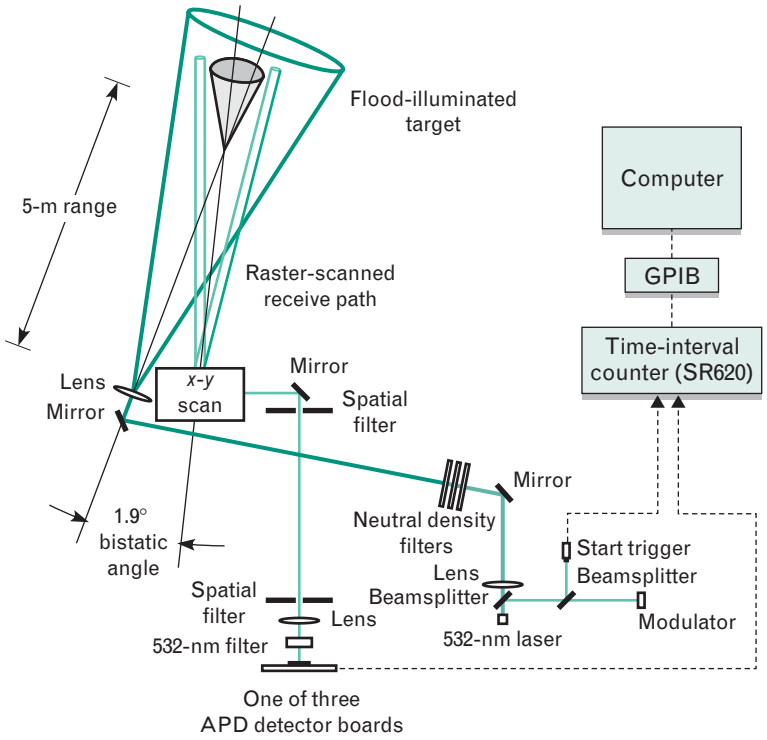

FIGURE 4. Diagram of setup that proved the feasibility of photon-counting 3D imaging. A Lincoln Laboratory–built microchip laser was used to flood-illuminate an indoor scene with short pulses of less than 1 nsec FWHM. Attenuating filters reduced the laser intensity so that the detector was receiving on average less than one photon per pulse. The laser-pulse transmit time was measured with a second optical detector and used to start the high-precision time-interval counter. Two single-axis scan mirrors were used to raster-scan the receive field of view over the target scene. One laser pulse was transmitted for each image pixel or receiver pointing location. A narrowband spectral filter reduced background light reaching the detector. We performed separate tests with three different APD detector boards: the dual-mode detector module (MIT-1), a commercial Single Photon Detection Module (SPCM) from EG&G Canada, and a single element of an experimental 4 × 4 detector array from Radiation Monitoring Devices, Inc. A computer was used to control and interface to the time-interval counter (Model SR620 from Stanford Research) through a general-purpose interface bus (GPIB, or IEEE-488 standard).

technology for efficient 3D imaging, and indicated that this method of 3D imaging is an enabling technology for remote sensing and automatic target recognition [8].

Microchip Lasers

Passively *Q*-switched microchip lasers are constructed by diffusion-bonding a short piece of laser-gain medium, in this case Nd:YAG, to a similarly short piece of saturable absorber, in this case chromium-doped YAG (Cr^{4+}:YAG) [9, 10]. The pump-side face of the composite structure is coated to transmit the pump light (808 nm from a diode laser) and reflect the laser light (1064 nm). The output face, which is coated to be partially reflecting at the lasing frequency, provides both feedback and laser output. The devices, typically a few millimeters long, are longitudinally pumped with the output of a multimode optical fiber. The pump diode is at the opposite end of the fiber. Figure 7 shows the simplest embodiment of the laser. In operation, the intracavity saturable absorber prevents the onset of lasing until the average inversion density within the cavity reaches a critical threshold. At that point, the onset of lasing produces a high intracavity optical field that saturates the absorber, resulting in a *Q*-switched output pulse a few hundred picoseconds long. The pulse repetition rate depends on pump power and is typically several thousand per second. The output beam has a transform-limited frequency spectrum, fundamental transverse mode with diffrac-

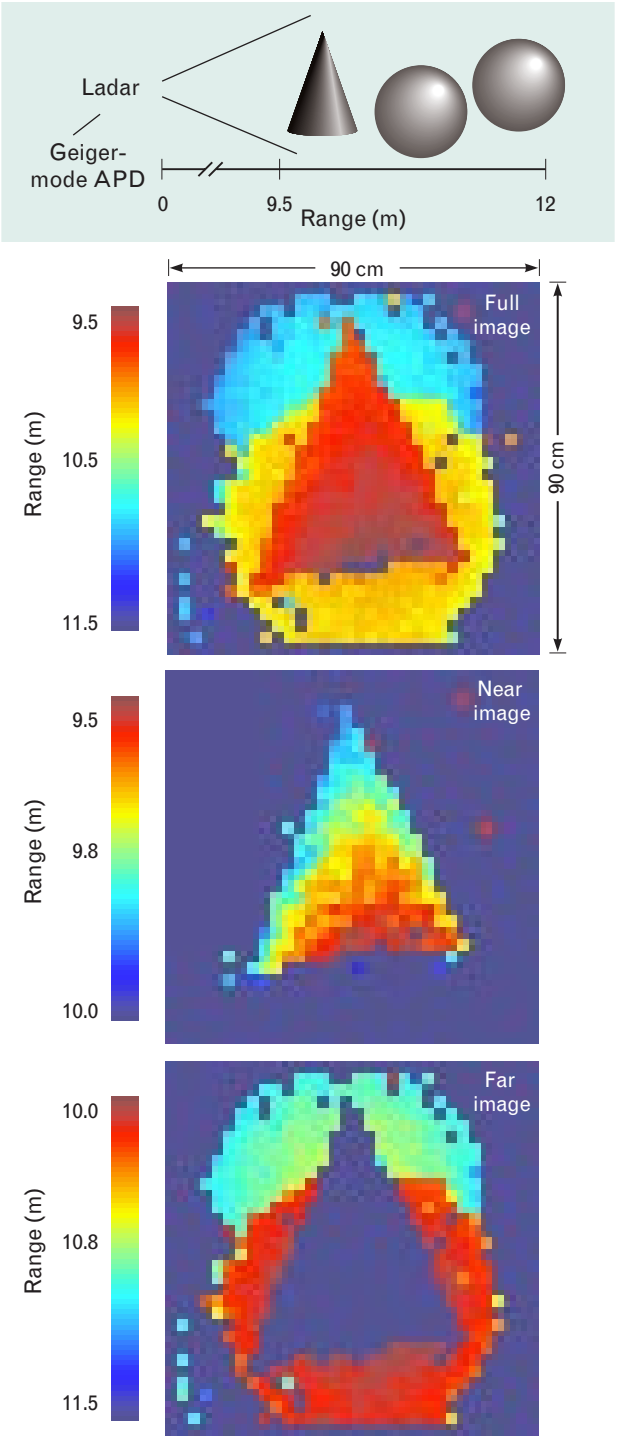

FIGURE 5. 3D ladar images of a cone and two spheres, taken in the laboratory by transmitting multiple flood-illuminating laser pulses while scanning the field of view of a single commercial APD operated in Geiger mode. The lower two images show how a simple thresholding operation applied to the measured range data can be used to segment the image, excluding either the more distant objects or the closer ones.

tion-limited divergence, and linear polarization.

For high pulse energies, the input and output faces of the composite structure shown in Figure 7 are capped with short pieces of undoped YAG in order to increase the damage threshold [11]. In separate devices, we have obtained 250 μJ per pulse at 1000 pulses/sec and 110 μJ per pulse at 5000 pulses/sec. Both lasers had 380-psec pulse widths. If higher energy is required at the same short pulse width, the output from such lasers can be coupled to optical amplifiers.

The high intensity of the output beam allows its frequency to be doubled by simply placing a small piece of titanate phosphate (KTP) near its output face. The energy efficiency of frequency doubling to the green (532 nm) is typically 50 to 60% [9–11]. If desired, a second nonlinear crystal adjacent to the first can convert the green light to ultraviolet at 355 or 266 nm [12], with an expected energy efficiency of about 25%. The addition of a small lens ahead of the second crystal can improve green-to-ultraviolet energy efficiency to about 50%.

Arrays of Geiger-Mode APDs Integrated with CMOS Timing Circuitry

The basic structure of the detector arrays [3, 6, 7], shown in Figure 8, consists of a two-dimensional array of APDs bonded to a commensurate array of timing electronics. The APDs are fabricated in Si and have a circular active area with a diameter of 30 to 50 μm and a pitch of 100 μm. The pitch is determined by area requirements of the timing electronics. The APDs are biased to operate in Geiger mode, in which an electron-hole pair generated by a single photon initiates an avalanche process that results in a large current pulse. This fast, high-amplitude current pulse triggers high-precision timing circuitry.

APD arrays with up to 32 × 32 detectors have been produced in several fabrication runs at the Lincoln Laboratory Microelectronics Laboratory. Measurements show that the 32 × 32 APDs have crosstalk of less than 1%, timing jitter of less than 150 psec, and 40% detection probability at 532 nm for uncoated, front-illuminated devices. Detection probability of about 80% is expected for optimally designed, anti-reflection-coated, backside-illuminated devices. The

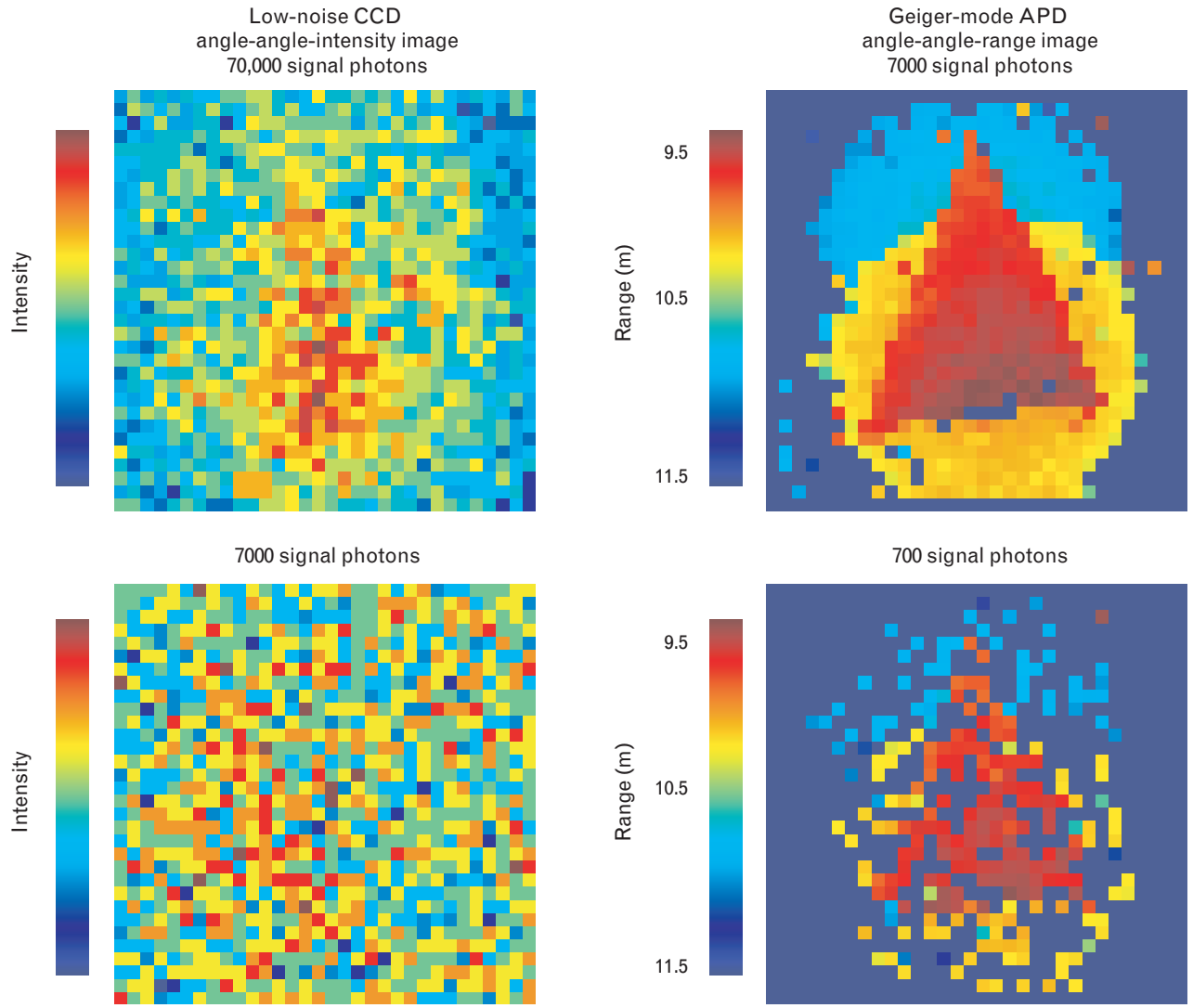

FIGURE 6. Comparison of angle-angle-intensity images (left) from a low-noise charge-coupled device (CCD) with spatial angle-angle-range images (right) from a 3D Geiger-mode APD, all of the same objects imaged in Figure 5. All images were obtained by active illumination of the scene by a laser, with the laser-pulse energy varied. The total number of detected photons in all 1024 pixels is indicated above each image. Note how much easier it is to recognize objects in the 3D APD images, even when the illumination is much less. All images have been normalized to identical quantum efficiencies.

measured dark-current rate of about 10 counts per msec is negligible for typical 3D-ladar applications; moreover, we expect to reduce it to about 1 count per msec with a different material-processing technique. A detailed description of these detector developments appears in the companion article by Aull et al.

Figure 9 is a block diagram of a 17-bit, single-pixel timing circuit. A common clock broadcast to all the pixels controls timing. The clock runs a feedback shift register that counts through a predetermined sequence. When the APD fires, the resulting signal triggers a latch, which stops the timing register. The data are then read out from each of the pixels in serial fashion. Also read out are two vernier bits representing the phases ϕ_1 of the master clock and ϕ_2 of a secondary clock, which is delayed in phase by 90° to provide higher temporal resolution. The first-generation devices produced in a 0.35-μm MOSIS CMOS process showed complete end-to-end operation down to 0.7-nsec timing resolution. The second-generation devices are expected to have resolution of 0.5 nsec or better [3, 6, 7].

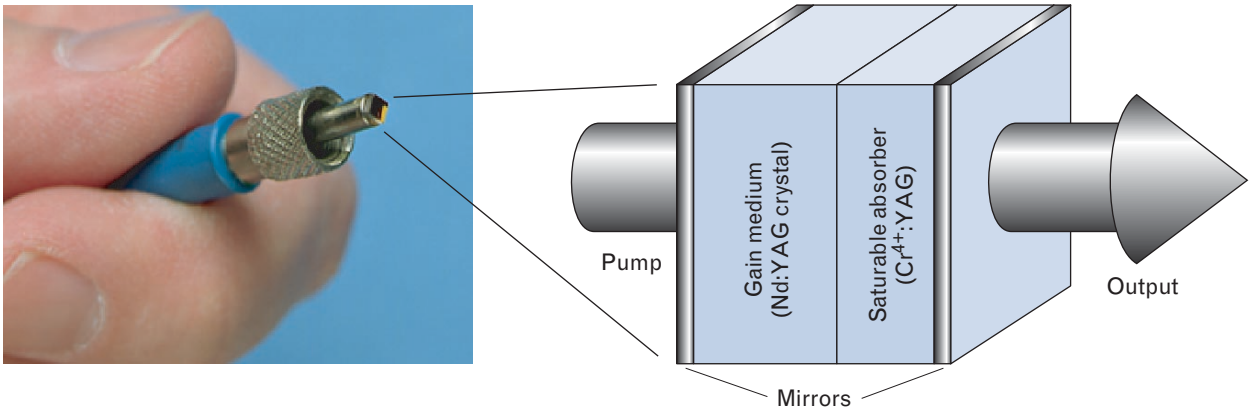

FIGURE 7. Simplest embodiment of passively *Q*-switched microchip laser. The microchip laser is attached to the end of an optical fiber, through which it is pumped with an 808-nm diode laser. The Nd:YAG (neodymium-doped yttrium aluminum garnet) crystal acts as the gain medium. The microchip laser is passively *Q*-switched by the saturable absorber of chromium-doped YAG (Cr^{4+}:YAG).

One of our major challenges is bonding the APD array to the timing-circuit array. We have developed a technique that we call bridge bonding. The CMOS chip is epoxied to the APD wafer, then sloped vias are etched through the epoxy and metallized to make an electrical connection between the APD and the timing circuit. An intermediate step, done after epoxying and before etching, is to thin the substrate of the APD wafer. Thinning enables the bridge-bonding process and is necessary to achieve a high detection probability, because the substrate is opaque to visible and near-infrared light. We have recently completed several integrated 32 × 32 APD/CMOS devices, and have developed working 32 × 32 arrays of detectors integrated with timing circuits. Scaling up to larger arrays should be straightforward.

3D-Ladar Brassboard

Lincoln Laboratory developed a transportable 3D-ladar system. This first-generation system, called a brassboard, was built to test the interaction of the various ladar components and to gather 3D images of full-scale targets for subsequent analysis.

Figure 10 shows a diagram of the optical layout of the brassboard. The pulsewidth is 380 psec. The 532-nm microchip laser emits 30 μJ per pulse at 1000

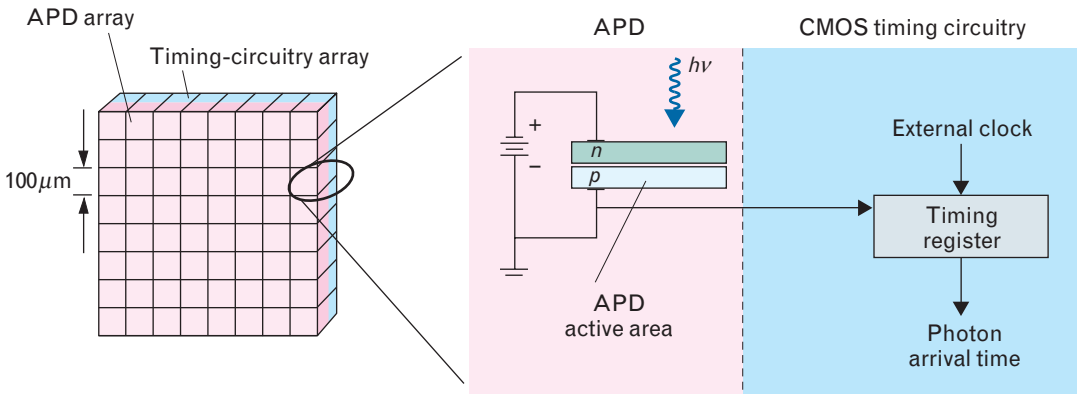

FIGURE 8. Basic structure of focal-plane array consisting of Geiger-mode APDs bonded to complementary-metal-oxide-semiconductor (CMOS) timing circuitry. A photon of energy $h\nu$ is absorbed in the APD active area. The gain of the APD resulting from the electron avalanche is great enough that the detector generates a pulse that can directly trigger the 3.3-V CMOS circuitry. No analog-to-digital converter is needed. A digital logic latch is used to stop a digital timing register for each pixel. The time of flight is recorded in the digital value of the timing register.

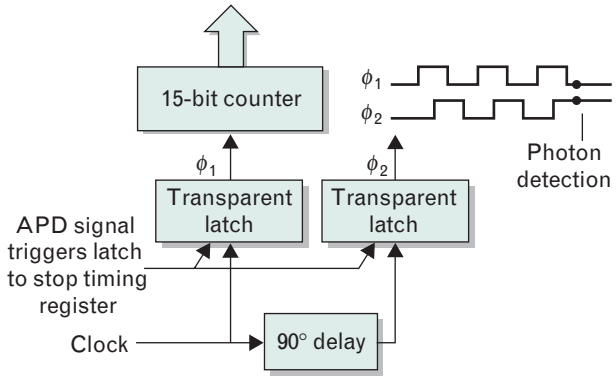

FIGURE 9. Block diagram of single-pixel timing circuit with 17-bit resolution. A common clock broadcast to all the pixels controls timing. The clock runs a feedback shift register that counts through a predetermined sequence that uses a 15-bit counter. When the APD fires, the resulting signal triggers a latch, which stops the timing register. Data are then read out from each of the pixels in serial fashion. Also read out are two vernier bits representing phases ϕ_1 of the master clock and ϕ_2 of a secondary clock, which is delayed in phase by 90° to provide higher temporal resolution.

pulses/sec. The Geiger-mode APD detector array is a 4 × 4 prototype. The timing electronics are external (not integrated) and have a least-significant bit of 75 psec. Separate time-to-digital converters measure the times of the outgoing laser pulse and of the APD current pulse. We have measured single-pixel range precisions of 2.0 cm at high detection probabilities. The 4 × 4 array is scanned across a target to generate images up to 128 × 128 pixels. The frame rates for 32 × 32 and 128 × 128 images are 4.5 per sec and 0.6 per sec, respectively. The adjustable range gate (i.e., the recording interval beginning when the APDs are overbiased to Geiger mode) is typically 100 nsec and starts at a selectable time after the laser pulse is detected in the transmit optical path. The entire system fits into a van and can be taken to field sites.

To date, a variety of static and dynamic images of people, cars, trucks, planes, boats, trees, wires, foliage, and other objects have been collected with the brassboard. Figures 11 through 13 show examples of these

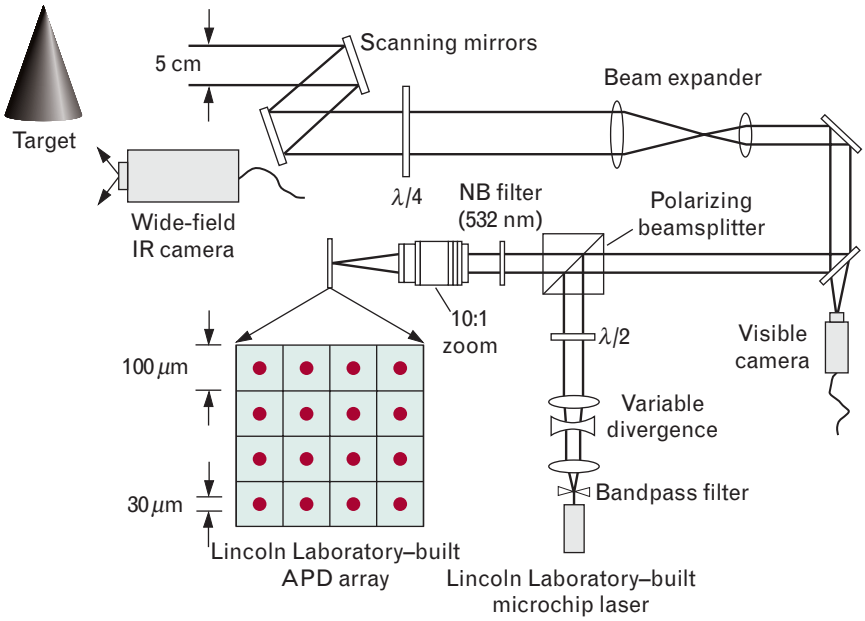

FIGURE 10. Diagram of the optical layout of the brassboard developed to test the 3D-ladar concept. A Lincoln Laboratory–built microchip laser transmits short pulses to a target scene. The laser beamwidth is matched to the instantaneous field of view of a 4 × 4 Geiger-mode APD array with 100-μm pitch and 30-μm active diameter. Two single-axis scan mirrors raster the 4 × 4 instantaneous field of view over the target field of regard to generate images with up to 128 × 128 pixels. The outputs of the sixteen detectors are recorded for each laser pulse. A narrowband (NB) filter reduces background light falling on the detector array. A polarizing beamsplitter serves as a transmit-receive switch. Infrared and visible-based cameras are auxiliary sensors.

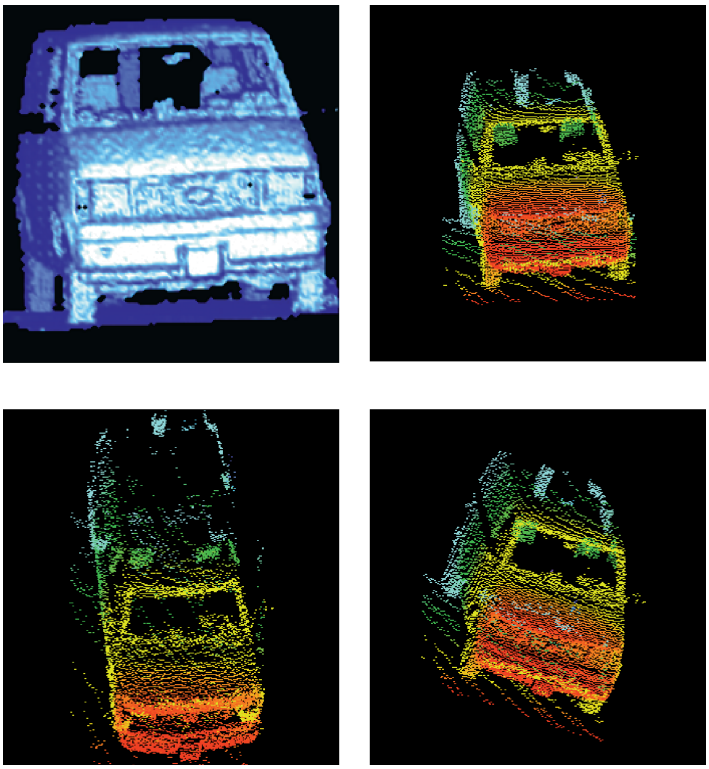

FIGURE 11. Image of a Chevrolet Astro van obtained from the 3D-ladar brassboard. This is a single 128 × 128-pixel image recorded with the ladar looking at the front and right side of the van from a distance of 60 m. In the upper left is a 3D model rendered from the angle-angle-range data. The other three renditions are point clouds that have been computer-rotated to view the van from different aspects. In a point cloud, each pixel is assigned a point with *x*- and *y*-coordinates corresponding to the pixel position in the array and a *z*-coordinate corresponding to its range. The points, colored according to range, are then projected onto a plane representing the viewing screen. Rotating the image in software better reveals shapes, sizes, and relative positions of different parts of the van.

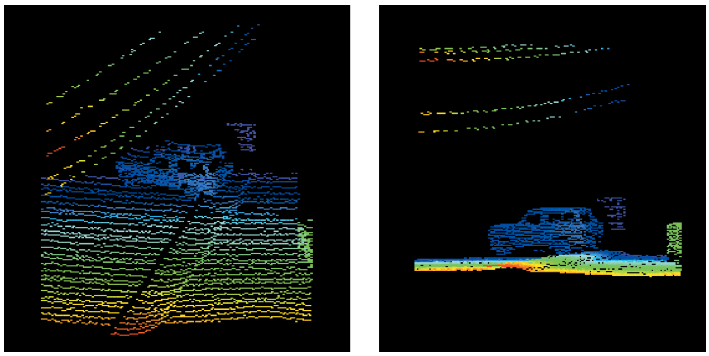

FIGURE 12. 3D image of a Ford Bronco with overhead wires shown after two different rotations. The 3D position of the wires with respect to the Bronco and to the brassboard can be determined from the angle-angle-range data.

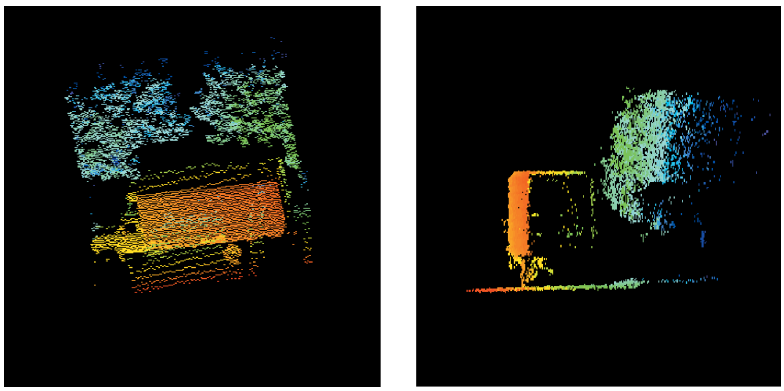

FIGURE 13. 3D image of a truck in front of two trees. Laser light penetrated the outer envelope of the trees. The point cloud is shown after two different amounts of computer rotation to better reveal the 3D structure of the trees.

images, which were all recorded in the daytime from a single viewing point. The 3D quality of the images, which is difficult to appreciate from these 2D projected renderings, is enhanced when they are rotated in software and displayed dynamically on a monitor. With the 3D data, we can determine the separation of the headrests from the back door of the van of Figure 11, the relative positions of the overhead wires in Figure 12, and the 3D structure of trees in Figure 13.

Comparison of 3D and Intensity Images

As shown in Figure 6, targets can sometimes be better recognized from 3D images than from intensity images. This was demonstrated further in a series of measurements using the 3D-ladar brassboard and a low-noise CCD camera, both looking at the same scene. For all of the results presented here, the sensors were co-located and had the same field of view, and both provided image frames composed of 128 × 128 pixels.

The Lincoln Laboratory–built CCD camera has very low noise, only five to six electrons root mean square (rms) per pixel at our operating conditions. Its signal is digitized to 12 bits, with the least-significant bit corresponding to fewer than 5 electrons. For recordings of the camera images, the scene was illuminated by a 1-W, continuous-wave (CW), 808-nm diode laser. At this wavelength, the quantum efficiency of the camera is 55%.

For camera and ladar images that are presented later, we calculated the average number of photoelectrons created per pixel per frame. For the camera, we used the measured calibration factor between number of photoelectrons and digital counts. For the ladar, we determined the detector firing rate for a given pixel and converted that to average number of photoelectrons by using the probability for a Poisson process.

Figure 14 shows the first results—both intensity and 3D images of a cone and a cylinder (with surrounding mounting structure) viewed nearly head on over a 65-m indoor range. Each image is from a single recorded frame. Because the camera has a 12-bit dynamic range, whereas displayed gray scale has only 8 bits, we show a single intensity image in three ways; namely, with (from left to right) the lower, middle, and upper 8 bits of the data mapped into the gray scale. Even with three versions of the intensity image, it is difficult, if not impossible, to tell what the objects are. In contrast, the shapes are evident from the 3D image, which also is shown in three different versions, as described in the figure caption. The 3D image was made with a very low 2.2 photoelectrons per pixel on average, and the intensity image at the top was made with 869 photoelectrons per pixel on average. Therefore, the ladar image was made with a signal lower by a factor of 400. Even so, it better reveals the shapes of the cylinder and cone.

Next, the sensors were placed about 10 m above ground level in the dome of the Lincoln Laboratory Firepond facility in Westford, Massachusetts. The intensity camera looked through an aperture only a few inches from that of the 3D-ladar brassboard. Another

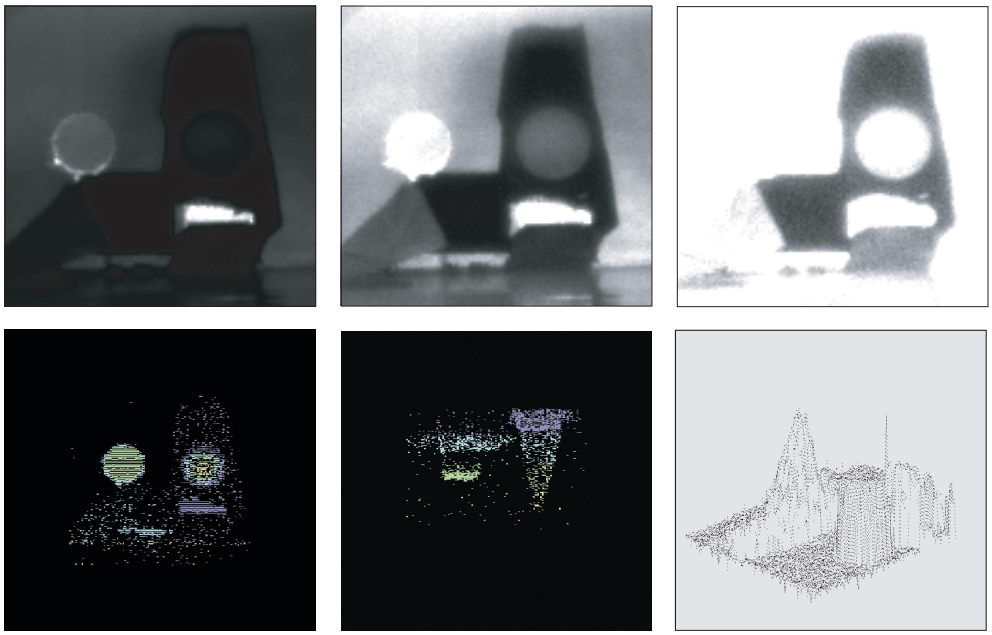

FIGURE 14. Intensity (top) and 3D (bottom) images of cone and cylinder viewed nearly head on, with mounting structure behind. These are single-frame images displayed in different ways. The 12-bit intensity image is shown (from left to right) with the lower, middle, and upper eight bits mapped into the 8-bit gray scale available from the printer. The 3D image at lower left is shown as a point cloud in its originally recorded orientation, with color coding according to range. At lower middle, the same 3D image is shown after computer rotation to show the view as if from above. At lower right is a surface-plot version of the 3D image with a different amount of computer rotation. Although the average number of photoelectrons per pixel is 869 for the intensity image and only 2.2 for the 3D-ladar image, the 3D image more readily reveals the shape difference between the cylinder and cone.

FIGURE 15. Photographs of the 500-m propagation range at the Lincoln Laboratory Firepond facility in Westford, Massachusetts. On the left is an aerial view with the Firepond dome at top right and the target pad at bottom right. The middle image shows the view from the dome toward the target pad, and the right image shows the view from the pad to the dome. The 3D-ladar brassboard, low-light-level intensity camera, and diode laser were housed within a few inches of one another in the dome. At nighttime, the diode laser illuminated the scene for the camera.

FIGURE 16. Photographs of objects imaged by the ladar and camera. The van has a pod on top, the utility vehicle is camouflage painted, the net is camouflage colored, and the trees are evergreens.

few inches away was the aperture of the 808-nm diode laser that illuminated the scene for the camera. The sensors looked at objects placed at the far end of a 500-m path that was cleared of trees and brush, as shown in Figure 15.

In a typical setup at the 500-m site, two vehicles were arranged side by side, slightly facing one another and seen nearly head on from the dome. A few meters in front of one of the vehicles was either a camouflage net or a line of evergreen trees. The trees were freshly cut and were leaned against a suspended rope. Figure 16 shows the vehicles, camouflage net, and trees. The camouflage net is colored in drab shades of green and brown.

The fields of view of the 3D ladar and intensity camera were aligned to each other and were about 9 m across at the 500-m site. Because each sensor has 128 × 128 pixels, each had a pixel size of about 7 cm. The diffraction-limited resolution for the sensors, which had receiving apertures of about 5 cm, was about 1 cm. The diode laser for the camera illuminated a circular area with a diameter of about 9 m. The range gate of the 3D ladar, about 15 m deep, encompassed the scene of interest. For each 500-m setup, we recorded 100 to 200 frames of data from each sensor.

In Figures 17 and 18, the images are presented after multiple-frame processing. To process the camera data, we averaged N frames (i.e., averaged the N values for each pixel) and displayed the average frame with an 8-bit gray scale. The intensity range of the data does not exceed 8 bits. We tried various mappings of intensity into gray scale in an attempt to reveal the details of interest. (The signal-to-noise ratio obtained by averaging 200 camera frames recorded over a time t is lower than that which would be obtained by allowing the camera to integrate for the entire time t before reading out a single frame. The reason for this is that readout noise is suffered 200 times instead of only once. Even so, the data show that actual signal-to-noise ratios were very high and were not the factors limiting recognizability of imaged objects.)

For the 3D ladar, we recorded N frames and then created a range histogram for each pixel. A range histogram is a graph of the number of times that each range is measured versus range. The range scale was divided into bins of width 1.1 cm, the size of the

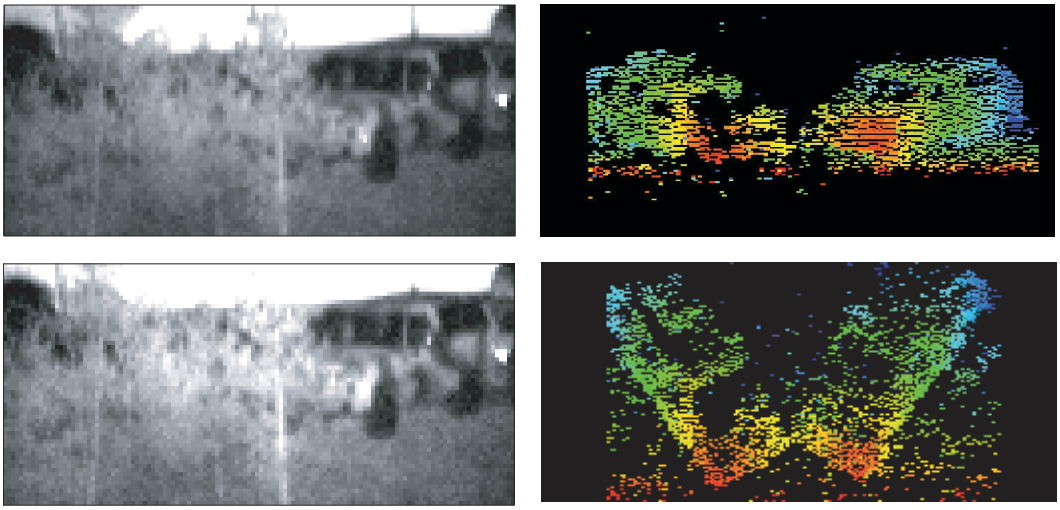

FIGURE 17. Intensity (left) and 3D (right) images of an exposed, camouflage-painted utility vehicle and a line of trees behind which is the white van. The intensity image is shown with two different mappings of intensity to gray scale, and the 3D image is shown after computer rotations by two different angles. One hundred frames recorded on a moonless night were processed. The average number of photoelectrons associated with the right-side utility vehicle is roughly 600 per pixel per frame for the intensity image and 0.05 per pixel per frame for the 3D image. Even so, the 3D image reveals the white van with its rooftop pod behind the trees, while the intensity image fails to do so.

least-significant bit in the timing electronics. For a pixel imaging part of a solid object, the recorded ranges accumulated in the bin corresponding to the range to the object. A few neighboring bins also have data points because of timing jitter in the brassboard and because of the depth of the object within the pixel, if any. Other data points were scattered about in more distant range bins because of noise. We located the bin with the maximum number of data points and calculated the first moment of the range over an interval encompassing a few range bins on either side of the maximum bin. We took this moment as the object's range. When a particular pixel covered parts of two objects separated in range, the range histogram exhibited two peaks. In this case, we chose to display either peak or both.

Figure 17 shows intensity and 3D images of the camouflage-painted utility vehicle and white van. The van is a few meters behind the line of trees on the left side of the images, and the utility vehicle is on the right. One hundred frames recorded on a moonless night were processed.

For the intensity image on the left side of Figure 17, the average number of photoelectrons associated with the right-hand vehicle is roughly 600 per pixel per frame. The corresponding signal-to-noise ratio is approximately 1000, given that the noise is approximately 6 electrons and that the signal-to-noise ratio scales as the square root of the number of frames averaged. The camera image is shown with two different mappings of intensity to gray scale. The maximum and minimum intensities differ by 8 bits, and in the upper image all 8 bits are shown. In the lower image, the bottom 7.5 bits of the data are mapped into the 8-bit gray scale to provide more contrast in the tree region at the expense of saturation in other regions.

The range gate of the ladar was set to open between the trees and the van. For the 3D image, the number of photoelectrons associated with both vehicles is roughly 0.05 per pixel per frame on average, the attenuation by the trees being offset by the higher reflectivity of the van. The 3D image is shown after computer rotations of 10° (upper image) and 45° (lower image).

In Figure 17, the van behind the trees cannot be discerned in the intensity image, despite having an average signal-to-noise ratio of approximately 1000. Yet it can be readily discerned in the 3D-ladar image,

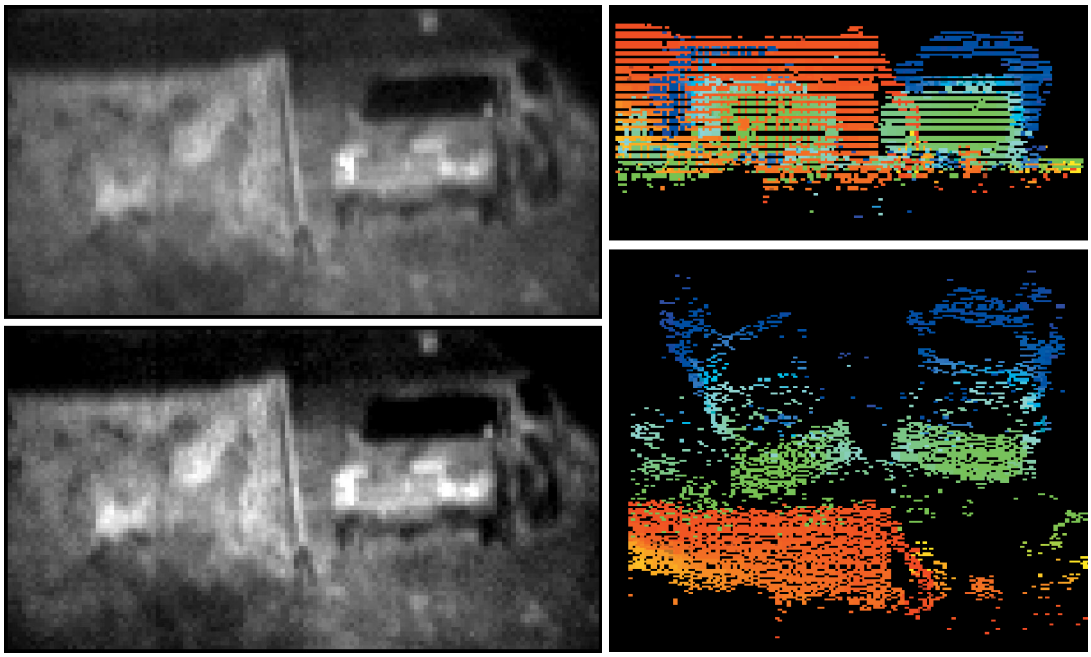

FIGURE 18. Intensity (left) and 3D-ladar (right) images of two camouflage-painted utility vehicles, one behind a camouflage net. The intensity image is shown with two different mappings of intensity to gray scale, and the 3D image is shown from two different aspect angles. Two hundred frames, recorded on a moonless night, were processed. The average number of photoelectrons associated with the right-side vehicle is roughly 120 per pixel per frame for the intensity image and only 0.4 per pixel per frame for the 3D image. The vehicle behind the net shows up clearly in the 3D image after computer rotation, but it cannot be discerned in the intensity image.

which was made with four orders of magnitude fewer photoelectrons than was the intensity image. The trees were thick enough in a few spots to block all laser light to the van, so the 3D image has a few holes in it. Even so, it is clear (especially when the point cloud is rotated via software) that a vehicle with a pod on top is behind the trees. The vehicle on the right clearly does not have a pod and has a different shape. The ability to create a high-quality 3D image with extremely low light levels attests to the exquisite sensitivity of the Geiger-mode APDs.

In Figure 18, the line of trees has been replaced by a camouflage net, and a second camouflage-painted utility vehicle is behind the net. We have conclusions similar to those above: the 3D image shows that the size and shape of the vehicle behind the net are the same as for the unobscured vehicle, while the intensity image, with two orders of magnitude more photoelectrons, fails to reveal even that a vehicle is behind the net.

In Figures 17 and 18, the vehicles behind the net and trees are difficult to recognize from the intensity images, even though signal-to-noise ratios are high. Part of the reason for this may be low intensity contrast between the vehicles and obscurants. Low contrast can be caused by similar reflectivities at the sensed wavelength (808 nm) and by the mixing within a pixel of photons from both the obscurant and the vehicle. Contrast might have been better if some other wavelength had been used, or if multiple wavelengths and special processing had been used, or if the pixels had been smaller to reduce mixing. Also, higher signal-to-noise ratios and finer intensity resolution in displays would help distinguish low-contrast objects. Perhaps more important than low contrast in limiting recognizability are the spatial variations in intensity impressed upon the image by the obscurant. The variations have spatial frequencies similar to those of features on the vehicles and thereby hide the distinguishing features. The 3D data do not suffer

from these limitations; they are insensitive to intensity contrast variations, and they provide range so that the transverse features of the obscurant and vehicle can be separated. In addition, the 3D data reveal size and shape. These characteristics of the 3D data make the vehicles recognizable in the 3D images even when the signal levels are much lower than those for the intensity images.

Future Development of 3D Ladar

We are currently developing more compact 3D imaging ladar systems, which will use the recently developed 32 × 32 APD/CMOS arrays [2]. Given success with this size, we expect that scaling up to 128 × 128 elements or greater will be straightforward.

Because the quantum efficiency of Si detectors decreases rapidly for wavelengths beyond about 900 nm, we are developing APDs with Class III-V semiconductor materials that will respond to longer wavelengths, such as those around 1500 nm in the eye-safe regime.

The energy per pulse (up to approximately 100 μJ at 532 nm) and repetition rate (greater than 1000 pulses/sec) from existing microchip lasers are sufficient for many applications. If an application requires more energy, it is straightforward to couple a microchip laser to a diode-pumped, solid-state amplifier. Eye-safe wavelengths around 1500 nm can be produced by using microchip lasers to pump optical parametric oscillators [13].

With microchip lasers and microelectronic arrays of detectors and timing circuitry, we expect that an entire 3D ladar can fit into a package small enough (the size of a coffee can) and light enough (two or three kilograms) to be handheld. Because the ladar could work at greater than 1000 frames per second, hundreds of frames could be processed in a fraction of a second in order to see through obscurants, to freeze motion in a dynamic scene or in the ladar platform, or to extend the range. The range can also be greatly extended by coupling the microchip laser to an amplifier. After development, such a ladar could operate at an eye-safe wavelength near 1500 nm. As shown by the images in this article, a 3D-imaging ladar with Geiger-mode photon-counting arrays can provide valuable target and scene information at very low signal levels. This information is difficult to obtain from intensity cameras at even much higher signal levels.

Acknowledgments

In addition to the authors, many others have contributed to the development and maturation of these novel and interesting imaging technologies. Paul F. McManamon of the Air Force Research Lab Sensors Directorate and Walter Dyer of the Missile Defense Agency were early supporters of this activity and helped initiate the pioneering concepts and experiments. The MIT Lincoln Laboratory Advanced Concepts Committee provided support for the early laboratory experiments in 3D imaging with photon-counting detectors (ACC Project 199). Through their careful and creative efforts, Salvatore DiCecca, Juan Ochoa, and Antonio Rubio-Sanchez assembled and operated the first laboratory proof of principal. The first 3D ladar images from an array of detectors were accomplished with generous support from Stephan Vasile, then of Radiation Monitoring Devices, Inc., who provided samples of his novel 4 × 4 silicon Geiger-mode APD arrays for testing. These encouraging results have led to Lincoln Laboratory development of the brassboard ladar system as well as the 4 × 4 and 32 × 32 arrays of detectors and digital timing circuits described in the companion article in this issue by Brian F. Aull, et al. We also acknowledge the support from DARPA, SDIO, BMDO, and the U.S. Army, U.S. Navy, and U.S. Air Force.

REFERENCES

1. J.J. Zayhowski, "Microchip Lasers," *Linc. Lab. J.* **3** (3), 1990, pp. 427–446.
2. B.F. Aull, A.H. Loomis, D.J. Young, R.M. Heinrichs, B.J. Felton, P.J. Daniels, and D.J. Landers, "Geiger-Mode Avalanche Photodiodes for Three-Dimensional Imaging," *Linc. Lab. J.*, in this issue.
3. W.E. Keicher, W.E. Bicknell, R.M. Marino, T. Stephens, W.R. Davis, and S.E. Forman, "Laser Radar Technology for Ballistic Missile Defense," *Linc. Lab. J.* **13** (1), 2001, pp. 205–228.
4. R.M. Heinrichs, B.F. Aull, R.M. Marino, D.G. Fouche, A.K. McIntosh, J.J. Zayhowski, T. Stephens, M.E. O'Brien, and M.A. Albota, "Three-Dimensional Laser Radar with APD Arrays," *SPIE* **4377,** 2001, pp. 106–117.
5. R.M. Marino, R.M. Spitzberg, and M.J. Bohrer, "A Photon Counting 3-D Imaging Laser Radar for Advanced Discriminating Interceptor Seekers," *2nd Ann. AIAA SDIO Interceptor Technology Conf., 6–9 June 1993, Albuquerque, N.Mex.*
6. B.F. Aull, A.H. Loomis, J.A. Gregory, and D.J. Young, "Geiger-Mode Avalanche Photodiode Arrays Integrated with CMOS Timing Circuits," Mtg. of the Boston Chap. of the IEEE Electron Devices Society, Lexington, Mass., Nov. 1998.
7. B.F. Aull, "Geiger-Mode Avalanche Photodiode Arrays Integrated with CMOS Timing Circuits," *56th Ann. Device Research Conf. Dig., Charlottesville, Va., 22–24 June 1998,* pp. 58–59.
8. R.M. Marino, "Method and Apparatus for Imaging a Scene Using a Light Detector Operating in Non-linear Geiger-mode," U.S. Patent No. 5,892,575 (6 Apr. 1999).
9. J.J. Zayhowski and C. Dill III, "Diode-Pumped Passively *Q*-Switched Picosecond Microchip Lasers," *Opt. Lett.* **9** (18), 1994, pp. 1427–1429.
10. J.J. Zayhowski, "Passively *Q*-Switched Microchip Lasers and Applications," *Rev. Laser Eng.* **29** (12), 1988, pp. 841–846.
11. J.J. Zayhowski, C. Dill III, C. Cook, and J.L. Daneu, "Mid- and High-Power Passively *Q*-Switched Microchip Lasers," *OSA TOPS* **26,** *Advanced Solid-State Lasers*, *Topical Mtg., 31 Jan.–3 Feb. 1999,* pp. 178–186.
12. J.J. Zayhowski, "Ultraviolet Generation with Passively *Q*-Switched Microchip Lasers," *Opt. Lett.* **21** (8), 1996, pp. 588–590; *errata*, *Opt. Lett.* **21** (19), 1996, p. 1618.
13. J.J. Zayhowski, "Periodically Poled Lithium Niobate Optical Parametric Amplifiers Pumped by High-Power Passively *Q*-Switched Microchip Lasers," *Opt. Lett.* **22** (3), 1997, pp. 169–171.

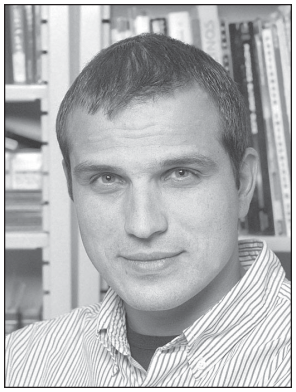

MARIUS A. ALBOTA
is an assistant staff member of the Optical Communications Technology group, researching nonlinear and quantum optics, optical communications, and imaging. Before this assignment, Marius was involved in the initial development and fielding of the 3D imaging laser radar with the Laser and Sensor Applications group. Prior to joining Lincoln Laboratory in 1997, he was a research assistant working on multiphoton microscopy at Cornell University. He received a B.S. degree in engineering physics from Cornell University and an S.M. degree in electrical engineering and computer science (EECS) from MIT. He is working on his Ph.D. degree in EECS at MIT through the Lincoln Scholars Program with advisors Franco N.C. Wong and Jeffrey H. Shapiro.

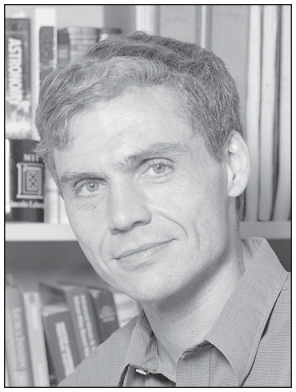

BRIAN F. AULL
develops 3D imaging and photon counting focal planes by using Geiger-mode avalanche photodiodes as a staff member in the Advanced Imaging Technology group. He joined the Laboratory in 1985, after earning a Ph.D. degree in electrical engineering from MIT. During his first decade at the Laboratory he led teams that demonstrated multiple-quantum-well spatial light modulators with gallium-arsenide/aluminum-gallium-arsenide (GaAs/ AlGaAs) charge-coupled device (CCD) arrays for electrical addressing and developed optoelectronic switching and neural processing devices by using quantum-well modulators and double-barrier resonant tunneling diodes. During the past two years Brian has developed arrays of Geiger-mode avalanche photodiodes integrated with high-speed CMOS timing circuits, which are being integrated into a 3D ladar system. He also holds a B.S. degree in electrical engineering from Purdue University.

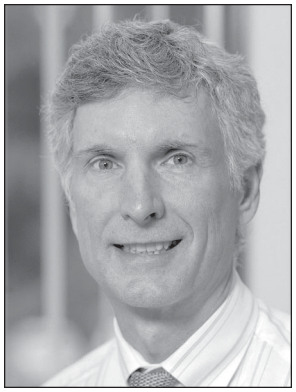

DANIEL G. FOUCHE
is a senior staff member of the Laser and Sensor Applications group. He joined Lincoln Laboratory in 1972 after receiving an A.B. degree in engineering and applied physics from Harvard University and a Ph.D. degree in applied quantum physics and quantum electronics from Yale University. His doctorate concerned inelastic light scattering from molecules. At the Laboratory, he has contributed to systems studies, hardware development, and experimentation in several electro-optical areas, including high-energy-laser propagation, precision tracking, adaptive optics, passive IR imaging, nonlinear optics, and laser ranging. Recently, he has focused on 3D imaging laser radars.

RICHARD M. HEINRICHS
leads the Laser and Sensor Applications group, which studies direct detection and coherent laser remote sensing. Rick joined Lincoln Laboratory in 1986, after completing a postdoctoral position in nonlinear fluid dynamics at the University of California in Santa Barbara. He received S.B. degrees in physics and electrical engineering and an S.M. degree in electrical engineering from MIT, and a Ph.D. degree in physics from the University of Massachusetts. He will chair the 2003 Coherent Laser Radar Conference.

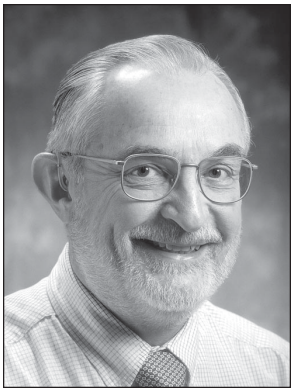

DAVID G. KOCHER received a B.S. degree in electrical engineering from the University of Illinois in 1957. Subsequently he received the S.M., E.E., and Sc.D. degrees in electronics from MIT. He joined Lincoln Laboratory in 1963 as a staff member, became a senior staff member in 1988, and currently is in the Laser and Sensor Applications group. At Lincoln Laboratory, he has specialized in electronic and optical instrumentation and measurements supporting three areas of defense-related research: optical measurement of missile reentry phenomena, the stabilization and control of high-energy laser beams, and the use of laser radars for remote sensing and measurement. In connection with this work, he has developed optical instrumentation for airborne sensors and for identifying the phenomena limiting the angular resolution of airborne telescopes. He developed an automatic optical focus sensor and a fifty-two-channel adaptive optics sensor for use with high-energy laser beams and led the teams that performed field tests of systems using these sensors. He also designed waveform generation and demodulation electronics for a wideband range-Doppler laser radar, receiver electronics for two single-photon detecting laser radars, and a laser illuminator used for missile tracking.

RICHARD M. MARINO received a B.S. degree in physics from Cleveland State University in 1979, and an M.S. degree in physics and a Ph.D. degree in high-energy physics from Case Western Reserve University in 1983 and 1985, respectively. In 1985 he joined Lincoln Laboratory as a staff member in the Laser Radar Measurements group. In 1993 he joined the Systems and Analysis group within the Air Defense Technology division. One of his most significant achievements has been his pioneering leadership in the development of a 3D imaging laser radar with photon-counting sensitivity. From 1995 to 1997 he worked at the Millimeter Wave Radar (MMW) and the ARPA-Lincoln C-band Observables Radar at the Kwajalein Missile Range in the Marshall Islands. While there, he was a mission test director at MMW and worked on Range Modernization Plans. In 1997 he joined the Sensor Technology and Systems group of the Aerospace division and relocated its Silver Spring, Maryland, location to join the National Polar-Orbiting Operational Environmental Satellite System (NPOESS)/Integrated Program Office (IPO). At the IPO, he was lead technical advisor for the NPOESS Cross-Track Infrared Atmospheric Sounder Instrument (CrIs). He returned to Lincoln Laboratory in Lexington in 1999 and is again working on the development of 3D imaging laser-radar systems.

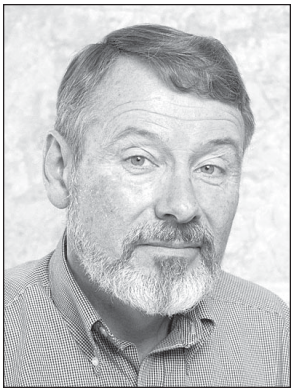

JAMES G. MOONEY is an associate staff member of the Laser and Sensor Applications group, working on analog and digital electronic design related to the detection of biological agents and 3D laser imaging systems. Jim joined the Laboratory in 1967 as an electronic technician. A year later, he joined the U.S. Navy and trained to work in electronic countermeasures. Returning to the lab in 1972, he worked on a number of adaptive optics systems used for high- energy laser propagation and atmospheric compensation.

NATHAN R. NEWBURY studies nonlinear effects in fiber optics for the Optoelectonics division at the National Institute of Standards and Technology (NIST). He previously worked at Lincoln Laboratory on biological agent detection and ladars. He earned a B.A. degree in physics from Williams College and a Ph.D. degree in physics from Princeton University.

MICHAEL E. O'BRIEN
is an associate staff member of the Laser and Sensor Applications group. His work focuses on the simulation of 3D laser radar systems and the processing of 3D laser radar data. He received a B.S. degree in mathematics from Rensselaer Polytechnic Institute and an M.S. degree in applied mathematics from Worcester Polytechnic Institute.

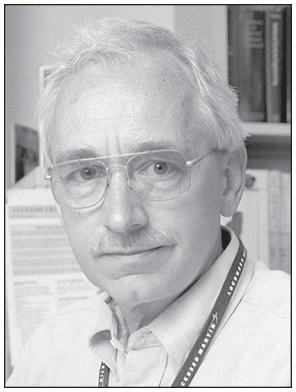

BRIAN E. PLAYER
supports the Laser and Sensor Applications group as subcontract engineer through Lockheed Martin. He specializes in optical detectors and preamplifiers used in direct detection and coherent laser remote sensing. Before joining the Laboratory as a subcontractor in 1974, Brian conducted radiometric measurements to support reentry physics for Avco Everett Research Laboratory in Everett, Massachusetts. He received a B.A. degree in physics from Northeastern University.

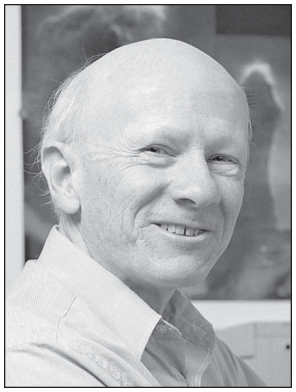

BERTON C. WILLARD
is a staff member of the Laser and Sensor Applications group, performing all of its optical systems engineering. His work focuses on 3D laser radars, laser vibrometers, adaptive optics, infrared imaging optics, and wake vortex monitors. He holds a B.S. degree in optics engineering and an M.S. degree in optics, both from the University of Rochester.

JOHN J. ZAYHOWSKI
is a senior staff member of the Quantum Electronics group, where he develops robust miniature solid-state laser systems and their applications. John holds fourteen U.S. patents in this area and has worked closely with industry to transfer the technology to the commercial sector. Applications enabled by John's work include the Lincoln Laboratory bio-aerosol warning sensor (BAWS) and high-resolution direct-detection 3D imaging ladar. John is a co-recipient of a 1998 R&D 100 award for the development of CyraxTM-Portable, 3-D Laser-Mapping and Imaging System. He is a member and former chairman of the Advanced Concepts Committee and a member of the New Technology Initiatives Board. John is the organizer and chairman of the subcommittee on Active Optical Sensing for the Conference on Lasers and Electro-Optics, to be held in Baltimore, Maryland, June 1–6, 2003; and the program chair for the Topical Meeting on Advanced Solid-State Photonics, to be held in San Antonio, Texas, February 2–5, 2003. Before joining the Laboratory in 1986, he worked for the Texas Instruments Central Research Laboratory in Dallas, Texas. John earned joint S.M. and S.B. degrees in electrical engineering and computer science and a Ph.D. degree in electrical engineering, all from MIT.